Moving Target Detection in Foliage Using Along Track Monopulse Synthetic Aperture Radar Imaging

Mehrdad Soumekh, *Member, IEEE*

***Abstract*—This paper presents a method for detecting moving targets embedded in foliage from the monostatic and bistatic Synthetic Aperture Radar (SAR) data obtained via two airborne radars. The two radars, which are mounted on the same aircraft, have different coordinates in the along track (cross-range) domain. However, unlike the interferometric SAR systems used for topographic mapping, the two radars possess a common range and altitude (i.e., slant range). The resultant monopulse SAR images are used to construct difference and interferometric images for moving target detection. It is shown that the signatures of the stationary targets are weakened in these images. Methods for estimating a moving target's motion parameters are discussed. Results for an ultrawideband UHF SAR system are presented.**

***Index Terms*—Foliage-penetrating SAR, monopulse SAR, moving target detection, Synthetic Aperture Radar (SAR).**

I. Introduction

UHF/VHF Synthetic Aperture Radar (SAR) systems have the ability to penetrate foliage, and obtain the SAR signature of concealed targets in foliage [1], [2], [20]. These radar systems, which are also known as foliage penetrating (FOPEN) SAR, are being investigated for detection of stationary and moving man-made targets in foliage. The task of detecting moving targets in foliage is particularly difficult. This is due to the fact that the image of a moving target in a reconstructed SAR image is smeared and weak as compared to the SAR image of the surrounding stationary foliage [3], [4], [17], [18]. Moreover, the foliage possesses a strong coherent signature that overlaps with the target signature in the frequency domain and, thus, it cannot be filtered out.

This paper introduces a monopulse SAR data collection and processing for moving target detection in foliage. A slant plane monopulse SAR system [see Fig. 1(a)] and an interferometric processing of the resultant images have been developed by Zebker and Goldstein [5] for topographic terrain mapping (see also [6]). The proposed monopulse SAR measurements for moving target detection are made by two radars that possess a common slant range but are separated in the along track (cross-range) domain [see Fig. 1(b)]. The coherent processing of the resultant along track monopulse SAR images carries information on the presence of moving target in the imaging scene.

Manuscript received July 18, 1995; revised July 23, 1996. This work was supported by the Office of Naval Research under Grant N00014-96-1-0586. The associate editor coordinating the review of this manuscript and approving it for publication was Dr. Charles V. Jakowatz, Jr.

The author is with Lincoln Laboratory, Massachusetts Institute of Technology, Lexington, MA 02173 USA, on leave from the Department of Electrical and Computer Engineering, State University of New York at Buffalo, Amherst, NY 14260 USA (e-mail: msoum@eng.buffalo.edu).

Publisher Item Identifier S 1057-7149(97)05478-X.

The roots of both slant plane monopulse SAR [5] and along track monopulse SAR, which is proposed in this paper, can be found in the classical radar analog/digital signal processing for height-finding and moving target detection with monopulse physical aperture radars [7]–[9]. An experimental phase-sum-and-difference monopulse radar was developed in as early as 1958 in the United States to detect moving targets in vegetative clutter [11, pp. 340–342]. Some of the extensions of this system are discussed in [12, ch. 5]. The main strength of slant plane and along track monopulse SAR's is in processing of high-resolution formed images to deduce information regarding terrain's altitude (slant plane monopulse SAR) or moving targets (along track monopulse SAR). There are unpublished works that utilize the classical monopulse radar processing on SAR data over short slow-time intervals for moving target detection. These methods are not applicable (degrade rapidly) when long slow-time intervals (coherent processing time in the slow-time) are used, which is the basis of the method that is outlined in the paper.

The reader will also find some common basic points between the along track monopulse SAR and short-pulse area Moving Target Indicator (MTI) [9] (the original work appears in [10]). In the case of short-pulse area MTI, the echoed signals due to several slow-time bursts (high range resolution) of a stationary monostatic radar are used for clutter filtering via noncoherent or coherent subtraction of successive radar video returns. (Similar principles have also been utilized in sonar signal processing to remove ship noise from passive sonar [13], Infrared Search and Track (IRST) [14], [15], and medical digital subtraction angiography [16].) For the airborne along track monopulse SAR, the foliage (clutter) does not appear at the same range at the various slow-time bursts of the moving transmitting radar. We will use a coherent processing of high-resolution formed images in the cross-range (along track) domain as well as range domain of an along track monopulse SAR system for moving target detection.

The paper is organized as follows. The monostatic and bistatic SAR signatures of a moving target with a constant speed for the along track monopulse SAR system are derived in Section II. In Section III, two methods for moving target detection using the monopulse SAR images are presented. One method is based on the difference of the two monopulse SAR images. The other method utilizes a phase comparison (an interferometric processing similar to the slant plane monopulse SAR) of the two along track monopulse SAR images. The effects of nonlinear motion and variations of terrain's altitude are analyzed in Section IV. It is shown that the along track monopulse SAR is also applicable for moving target

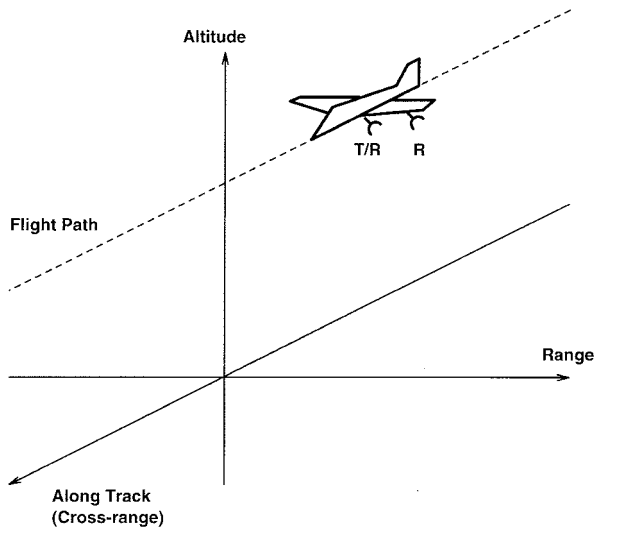

(a)

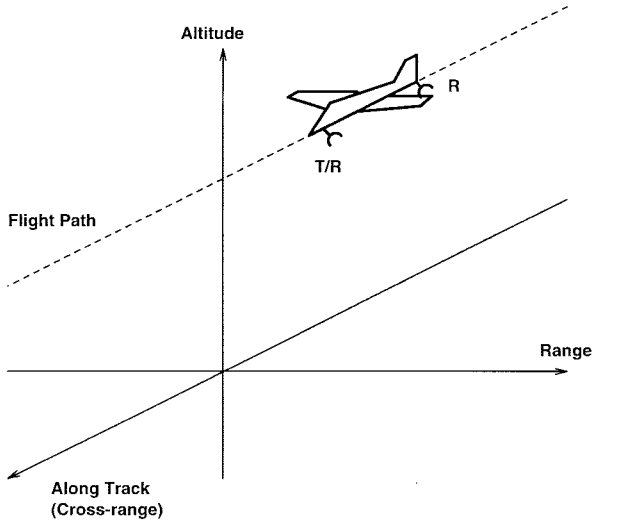

(b)

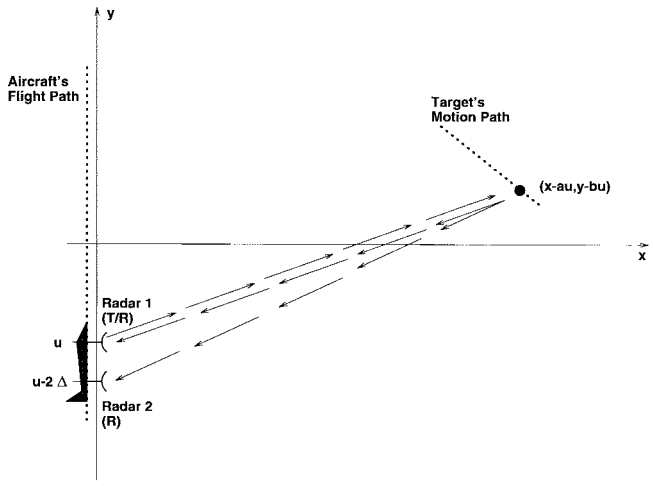

(c)

Fig. 1. Imaging system geometry for (a) slant plane monopulse SAR, (b) along track monopulse SAR, and (c) along track monopulse SAR in the ground plane.

detection in the realistic three-dimensional (3-D) slant plane reconnaissance SAR systems. The along track monopulse SAR data are used to estimate a moving target's motion parameters in Section V. The merits of the along track monopulse SAR system for moving target detection in foliage are examined for an ultra wideband UHF SAR problem.

II. Monopulse SAR Signal Model of a Moving Target

The along track monopulse SAR imaging system geometry in the two-dimensional (2-D) range (slant-range) and cross-range (x, y) domain is depicted in Fig. 1(c). We will examine this SAR problem in the 3-D spatial domain later. We denote the fast-time domain with t, and the synthetic aperture (slow-time) domain with u. The radar-carrying aircraft moves along the range $x = 0$.

A transmitting/receiving radar (Radar 1) illuminates the target area with a large-bandwidth pulsed signal $p(t)$. The resultant echoed signals are recorded by another receiving radar (Radar 2; bistatic SAR data) as well as Radar 1 (monostatic SAR data). (The two radars can be two subapertures of a single phased array.) Both radars have a common range (and altitude), i.e., $x = 0$. However, Radar 2 is separated by 2Δ from Radar 1 in the along track (cross-range) domain. Thus, at a given synthetic aperture position (slow-time) u, the coordinates of Radar 1 in the spatial domain is $(0, u)$, and the coordinates of Radar 2 in the spatial domain is $(0, u - 2\Delta)$.

We denote the speed of the airborne aircraft, which carries the radar with v_R. Suppose the velocity vector for a target is

$$(v_x, v_y) = (av_R, bv_R)$$

in the spatial (x, y) domain; (a, b), $|a|$, and $|b| \ll 1$, is the dimensionless target's velocity scaled to the speed of the radar, and is unknown.

A. Monostatic SAR

We start by developing the monostatic SAR signal recorded by Radar 1 due to the above-mentioned moving target. Let the spatial coordinates of the target at the slow-time $u = 0$ be (x, y); i.e., the target's motion path is $(x - au, y - bu)$ in the slow-time domain. Thus, the target's distance from Radar 1 at the slow-time u is

$$\sqrt{(x - au)^2 + [y - (1 + b)u]^2}.$$

In this case, the target's monostatic SAR signature in the (u, t) domain is

$$s_m(u, t) \equiv p\left[t - \frac{2\sqrt{(x - au)^2 + [y - (1 + b)u]^2}}{c}\right] \quad (1)$$

where $c = 3 \times 10^8$ m/s is the wave propagation speed. The Fourier transform of this echoed signal with respect to the fast-time t is [for notational simplicity, the fast-time Fourier transform of $s_m(u, t)$ is denoted with $s_m(u, \omega)$]

$$s_m(u, \omega) = P(\omega) \exp\left[-j2k\sqrt{(x - au)^2 + [y - (1 + b)u]^2}\right] \quad (2)$$

$$s_b(u,\,t) \equiv p\left[t - \frac{\sqrt{(x-au)^2+[y-(1+b)u]^2} + \sqrt{(x-au)^2+[y-(1+b)u+2\Delta]^2}}{c}\right] \tag{7}$$

where ω is the fast-time frequency domain, $k = \omega/c$ is the wavenumber, and $P(\omega)$ is the Fourier transform of the transmitted radar signal. For notational simplicity, we will not carry $P(\omega)$ in the following discussion.

The monostatic SAR signal in (2) can be rewritten as follows:

$$s_m(u,\,\omega) = \exp\left[-j2k\sqrt{r^2 - 2[ax+(1+b)y]u + [a^2+(1+b)^2]u^2}\right] \tag{3}$$

where $r \equiv \sqrt{x^2+y^2}$. Note that the target's motion trajectory can be uniquely identified via three parameters: r, $ax+(1+b)y$, and $a^2+(1+b)^2$. In fact, the target's motion trajectory with respect to the monostatic radar (Radar 1) can be expressed via the following:

$$\sqrt{X_m^2 + (Y_m - \alpha u)^2} = \sqrt{X_m^2 + Y_m^2 - 2\alpha Y_m u + \alpha^2 u^2}. \tag{4}$$

Equating (4) with the monostatic SAR signal in (3) yields

$$\begin{aligned} \text{Radial range:} \quad & \sqrt{X_m^2+Y_m^2} \equiv r \\ \text{Squint cross-range:} \quad & \alpha Y_m \equiv ax + (1+b)y \\ \text{Relative speed:} \quad & \alpha \equiv \sqrt{a^2+(1+b)^2}. \end{aligned} \tag{5}$$

Solving for (X_m, Y_m) from (5), it can be shown that the monostatic coordinates (X_m, Y_m) is a linear (rotational and scale) transformation of the (x, y); the parameters of the linear transformation depend on the target's motion parameters [17], [18], as follows:

$$\begin{aligned} X_m &\equiv \frac{(1+b)x - ay}{\alpha} \\ Y_m &\equiv \frac{ax + (1+b)y}{\alpha}. \end{aligned} \tag{6}$$

Note that for a stationary target, i.e., $(a,\,b) = (0,\,0)$, we have $(X_m,\,Y_m) = (x,\,y)$.

As we mentioned before, the speed of a moving target on the ground is much smaller than the radar-carrying aircraft, i.e., $|\alpha - 1| \ll 1$. In this case, the signature of a moving ground target in the reconstructed SAR image appears as a smeared structure around approximately $(X_m,\,Y_m/\alpha)$ which are defined in (6) [17], [18].

B. Bistatic SAR

At the synthetic aperture position u, the distance of the target from Radar 2 is

$$\sqrt{(x-au)^2+[y-(1+b)u+2\Delta]^2}.$$

Thus, the target's bistatic SAR signature, which is recorded by Radar 2, in the $(u,\,t)$ domain is shown in (7), at the top of the page. The Fourier transform of the bistatic SAR signal with respect to the fast-time t is

$$\begin{aligned} s_b(u,\,\omega) = {} & P(\omega)\exp\Big[-jk\sqrt{(x-au)^2+[y-(1+b)u]^2} \\ & -jk\sqrt{(x-au)^2+[y-(1+b)u+2\Delta]^2}\Big]. \end{aligned} \tag{8}$$

For the bistatic SAR signal, we will also not carry $P(\omega)$ in our discussion.

Suppose the target is stationary, i.e., $(a,\,b) = (0,\,0)$. In this case, provided that the distance of the two radars 2Δ is much smaller than the target's range r, the bistatic SAR measurements can be converted into monostatic SAR measurements of a transmitting/receiving radar, which is located at the midpoint of the line that connects Radar 1 and Radar 2 [19] as shown in the following:

$$\begin{aligned} \hat{s}_m(u,\,\omega) &\equiv s_b(u+\Delta,\,\omega)\exp\left(j\frac{k\Delta^2}{R}\right) \\ &\approx s_m(u,\,\omega) \end{aligned} \tag{9}$$

where R is the target area's mean range (radar's mean range swath). We refer to $\hat{s}_m(u,\,\omega)$ as the monostatic SAR signal which is synthesized from the bistatic SAR signal.[1]

The relationship in (9) can be established from the fact that the monostatic round trip distance

$$r_m(x,\,y,\,u) \equiv 2\sqrt{x^2+(y-u)^2} \tag{10a}$$

and the bistatic round trip distance

$$\begin{aligned} r_b(x,\,y,\,u) \equiv {} & \sqrt{x^2+(y-u)^2} \\ & + \sqrt{x^2+(y-u+2\Delta)^2} \end{aligned} \tag{10b}$$

are related via the following:

$$r_m(x,\,y,\,u) \approx r_b(x,\,y,\,u+\Delta) - \frac{\Delta^2}{2R}. \tag{11}$$

Thus, the reconstruction of a stationary target that is obtained from the monostatic SAR data $s_m(u,\,\omega)$, call it $f_m(x,\,y)$, is the same as the bistatic reconstruction, $f_b(x,\,y)$, that is formed from the synthesized monostatic data in (9).

The same, i.e., the relationship in (9), is not true for a moving target. We redefine the monostatic and bistatic round trip distances for a moving target via the following:

$$\begin{aligned} r_m(x,\,y,\,u) &\equiv 2\sqrt{(x-au)^2+[y-(1+b)u]^2} \\ r_b(x,\,y,\,u) &\equiv \sqrt{(x-au)^2+[y-(1+b)u]^2} \\ &\quad + \sqrt{(x-au)^2+[y-(1+b)u+2\Delta]^2} \end{aligned} \tag{12}$$

[1]The aircraft, which carries the radars, possesses a nonlinear motion component, call it $r_e(u)$ [18, Eq. (4.33)]. The nonlinear motion results in phase errors $\phi_m(u,\,\omega) = 2kr_e(u)$ and $\phi_b(u,\,\omega) = kr_e(u) + kr_e(u-2\Delta)$ in the monostatic and bistatic SAR signals, respectively. Provided that $r_e(u)$ is not a highly fluctuating signal (a condition which is met in practice), then (9) is still valid since $2r_e(u) \approx r_e(u+\Delta) + r_e(u-\Delta)$ and, thus, $\phi_m(u,\,\omega) \approx \phi_b(u+\Delta,\,\omega)$.

Then, using the fact that $\sqrt{a^2+b^2} \ll 1$ and $\Delta \ll R$, one can derive the following approximation:

$$r_m(x+a\Delta, y+b\Delta, u) \approx r_b(x, y, u+\Delta) - \frac{\Delta^2}{2R}. \quad (13)$$

Thus, the bistatic SAR data of the moving target corresponds to a spatial (x, y) domain shifted version of the monostatic SAR data of the same target (in addition to the shift of Δ in the synthetic aperture domain, which is also present for a stationary target). The amount of the shift in the spatial (x, y) domain, i.e., $(a\Delta, b\Delta)$, is related to the target's velocity, and is unknown.

If the monostatic SAR signal of a moving target is synthesized from its bistatic SAR signal via (9), we obtain the following:

$$\hat{s}_m(u, \omega) = \exp\left[-j2k\sqrt{(x+a\Delta-au)^2+[y+b\Delta-(1+b)u]^2}\right]. \quad (14)$$

The true monostatic SAR signal $s_m(u, \omega)$ and the synthesized monostatic SAR signal $\hat{s}_m(u, \omega)$ differ by the following phase function:

$$s_m(u, \omega)\hat{s}_m^*(u, \omega) \approx \exp\left[j2k\Delta\left(\frac{ax+by-bu}{R}\right)\right]. \quad (15)$$

Depending on the relative values of the target's parameters and the radar's frequency, this phase function can be significant or negligible.

The target's motion trajectory in the synthesized monostatic SAR signal of (14) can be expressed via the following:

$$\sqrt{X_b^2+(Y_b-\alpha u)^2}$$

where

$$X_b \equiv \frac{(1+b)(x+a\Delta)-a(y+b\Delta)}{\alpha} \approx X_m + a\Delta$$
$$Y_b \equiv \frac{a(x+a\Delta)+(1+b)(y+b\Delta)}{\alpha} \approx Y_m + b\Delta. \quad (16)$$

The signature of the moving ground target in the reconstructed SAR image appears as a smeared structure around approximately $(X_b, Y_b/\alpha)$.

Note that $(X_b, Y_b/\alpha)$ is a shifted version of $(X_m, Y_m/\alpha)$. The amount of this shift in the range and cross-range domains, i.e., $(a\Delta, b\Delta/\alpha)$, is smaller than the resolution in the range and cross-range domains for a practical SAR system. This is due to the fact that the monopulse radars are mounted on the same aircraft ($\Delta \ll R$), and the ground moving target's speed is much smaller than the radar-carrying aircraft's speed ($\sqrt{a^2+b^2} \ll 1$).

This is also the case for slant plane monopulse SAR, which is used for topographic terrain imaging, using monopulse radars that are mounted on the same aircraft (i.e., Δ is relatively small) [5]. In spite of this fact, as suggested by Zebker and Goldstein [5], interferometric processing of high-resolution slant plane monopulse SAR images yields the desired terrain altitude information (though the user faces the difficult task of 2-D phase unwrapping). In the next section, we use a coherent processing of along track monopulse SAR images for moving target detection.

TABLE I
PARAMETERS OF THE MOVING TARGETS

Target	x (m)	y (m)	v_x (m/sec)	v_y (m/sec)	α	X_m (m)	Y_m (m)
1	525	-80	4	4	1.053	528.3	-54.2
2	525	-70	0	4	1.052	525	-70
3	525	-60	4	0	1.001	527.4	-33
4	525	-125	6	8	1.106	532.5	-88

III. MOVING TARGET DETECTION

From (16), we can observe that the reconstruction of the moving target which is constructed from the synthesized monostatic SAR signal, $f_b(X, Y)$ at $(X, Y) \approx (X_b, Y_b/\alpha)$, appears shifted from its true monostatic SAR reconstruction, i.e., $f_m(X, Y)$ at $(X, Y) \approx (X_m, Y_m/\alpha)$. If the transmitted radar signal is a narrowband one (e.g., X band SAR) and the available values of u are much smaller than R, one can show from (15) that the two images approximately differ by the following phase function:

$$\exp\left[j2k_c\Delta\left(\frac{ax+by}{R}\right)\right] = \exp\left(j2k_c\Delta\alpha\frac{Y_m}{R}\right) \quad (17)$$

where k_c is the wavenumber at the carrier frequency. As we mentioned before, depending on the target's parameters and the radar's frequency, the phase function in (17) can be significant or negligible.

For an ultrawideband UHF SAR system, the difference between the two smeared reconstructions is more complicated than a simple phase function, and cannot be easily quantified. In our discussion, we use the narrowband models in (15) and (17) for the ultrawide band UHF SAR data for the lack of better references. The fact, however, remains that the two reconstructions have different phase and magnitude distributions, which could be significant depending on the target's parameters and the radar signal. Thus, the difference of the two reconstructions, i.e.,

$$f_d(X, Y) \equiv f_m(X, Y) - f_b(X, Y) \quad (18)$$

or the phase of the interferometric reconstruction, i.e.,

$$f_i(X, Y) \equiv f_m(X, Y)f_b^*(X, Y) \quad (19)$$

can be used to identify certain classes of moving targets.

In this paper, we present SAR reconstructions for a target scene that is illuminated with an ultrawideband UHF FOPEN radar signal. The radar signal's carrier frequency is 300 MHz, and its bandwidth is approximately 200 MHz. The aircraft speed is approximately $v_R \approx 80$ m/s. Four moving targets are simulated in a foliage area of this scene. The parameters of these targets are shown in Table I. All four moving targets possess a Gaussian beam pattern with standard deviation 50 m. The peak value of the simulated targets' SAR signature (i.e., the Gaussian beam) is chosen such that the resultant SAR image would have had approximately the same peak value as

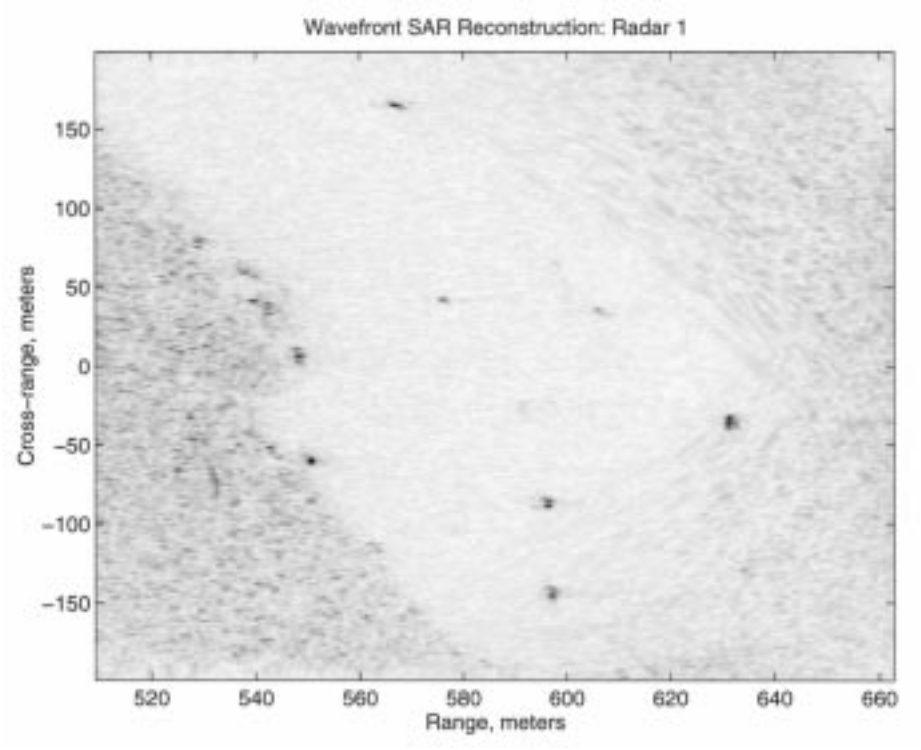

(a)

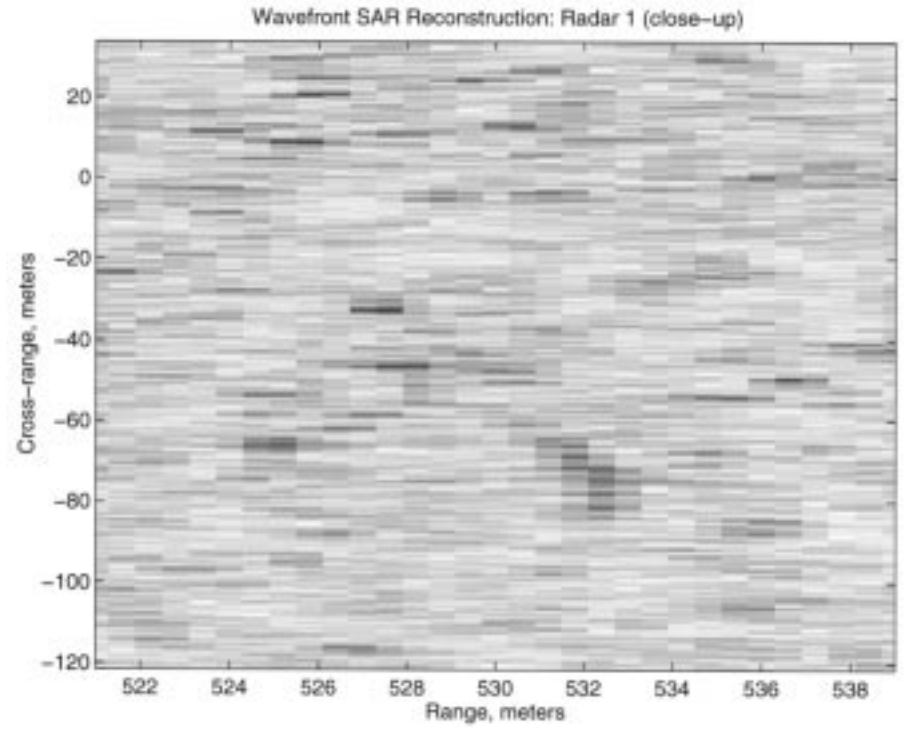

(b)

Fig. 2. Linear motion. (a) Monostatic SAR reconstruction. (b) Close-up of the area where the images of the four moving targets appear.

the surrounding trees if the targets had been *stationary*. Thus, the target-to-tree (coherent clutter) power ratio in the SAR image would have been 0 dB for a simulated stationary target. When the same beam pattern is used for a moving target, the target-to-tree in the SAR image gets smaller than 0 dB. This is due to the fact that a moving target SAR image appears shifted and smeared (less focused than a stationary target); this is discussed in details by Raney [3]. The amount of shift and smearing depends on the velocity (direction of motion as well as speed) of the target (see Raney [3] and [17]).

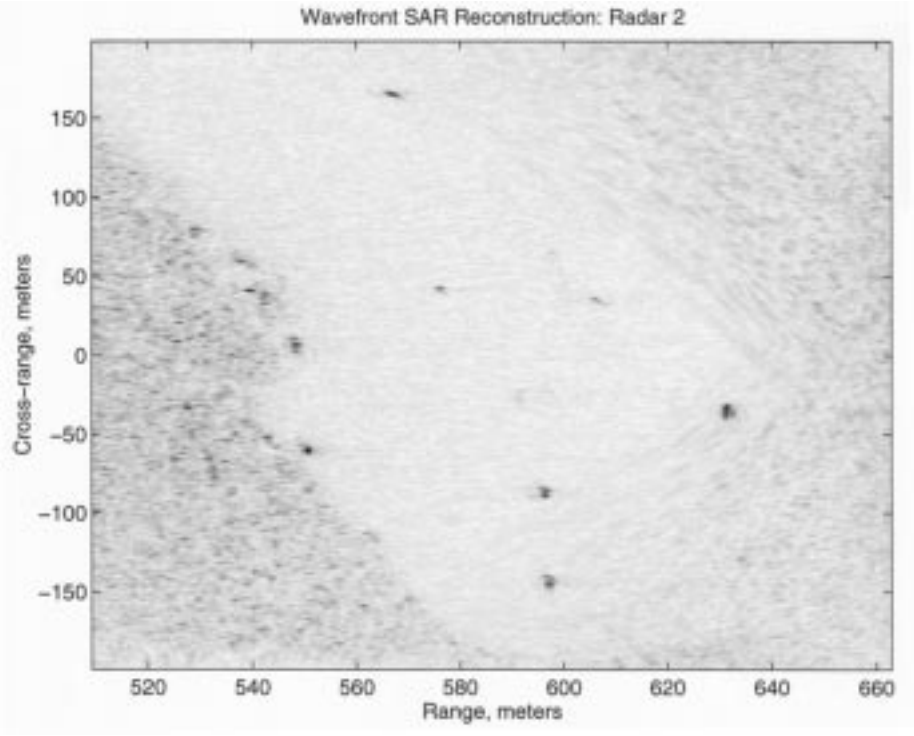

(a)

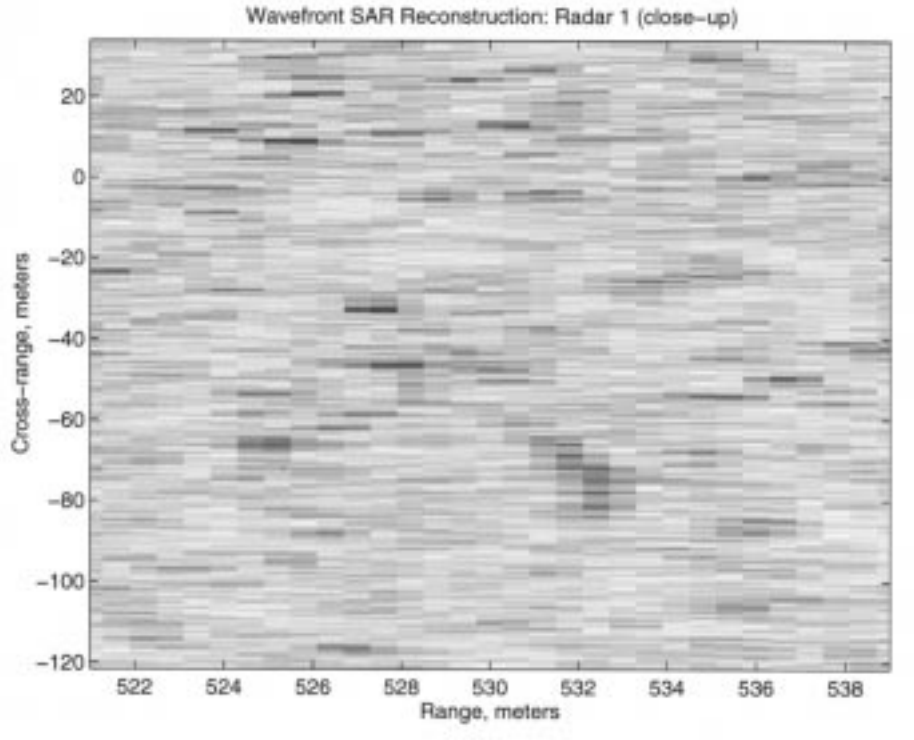

(b)

Fig. 3. Linear motion. (a) Bistatic SAR reconstruction. (b) Close-up of the area where the images of the four moving targets appear.

Figs. 2(a) and 3(a), respectively, show the monostatic (Radar 1) and bistatic (Radar 2) SAR reconstructions of the target area with $\Delta = 3.5$ m. Figs. 2(b) and 3(b) are the close-ups of these reconstructions at the area where the images of the four moving targets appear. Fig. 4(a) and (b) is the difference of the two reconstructions and its close-up, respectively. Fig. 5(a) and (b), respectively, shows the interferometric SAR phase (wrapped) and its magnitude for the close-up target area; the phase images are thresholded to show the pixel points where the magnitude of the reconstruction is above the 10% of the peak reconstructed value in the scene.

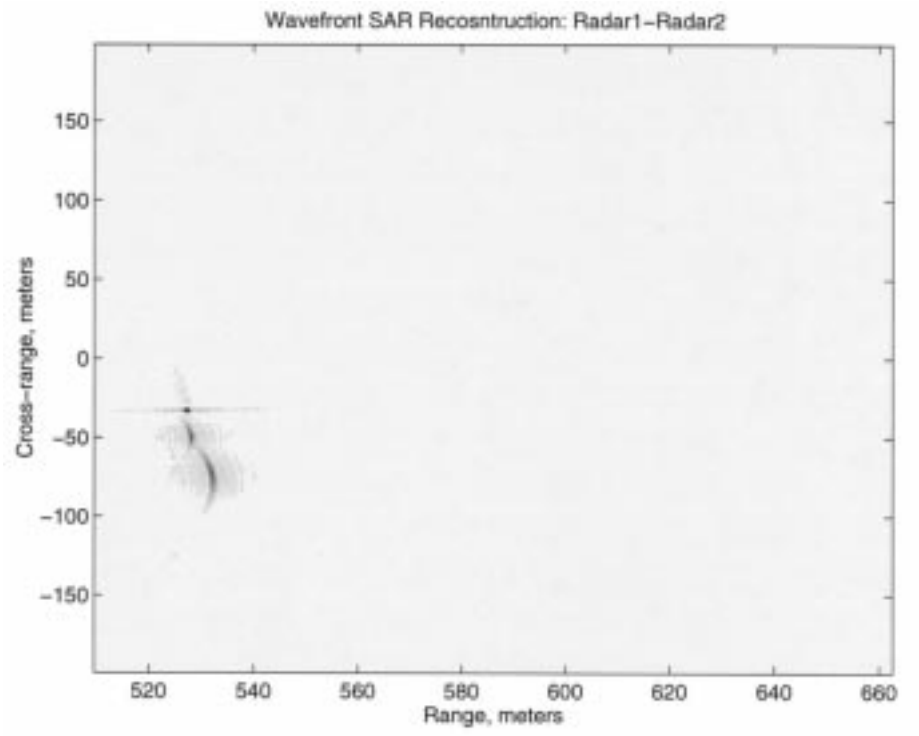

(a)

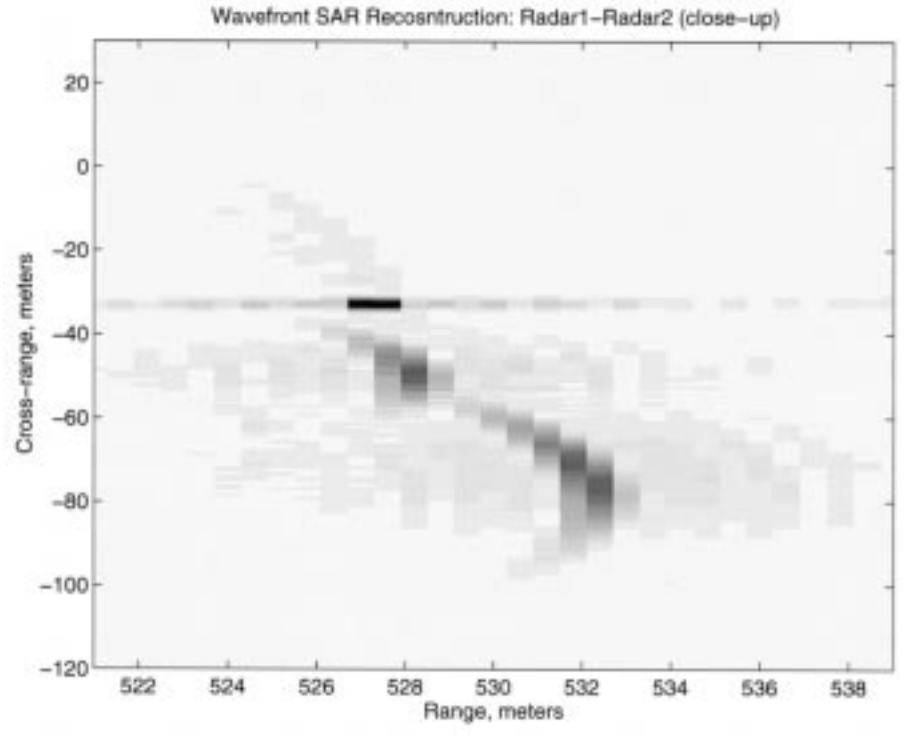

(b)

Fig. 4. Linear motion. (a) Difference SAR reconstruction. (b) Close-up of the area where the images of the four moving targets appear.

Depending on the relative velocity, the four moving targets exhibit different smearing effects and phase. Target 1, with $(x, y) = (525, -80)$ m, $(X_m, Y_m/\alpha) = (528.3, -51.47)$ m, and $(v_x, v_y) = (4, 4)$ m/s, appears as a smeared structure at the range $X = 528.5$ m and cross-range region $Y \in [-60, -40]$ m. This target appears in both Fig. 4 (difference reconstruction) and Fig. 5 (interferometric phase). This is mainly due to the nonzero value of v_x since the dominant phase term in (15) or (17) is due to ax; by is negligible.

This fact becomes evident in the reconstructions of Target 2 with $(v_x, v_y) = (0, 4)$ m/s. This target appears as a slightly smeared structure at $(X, Y) \approx (X_m, Y_m/\alpha) = (525, -66.5)$

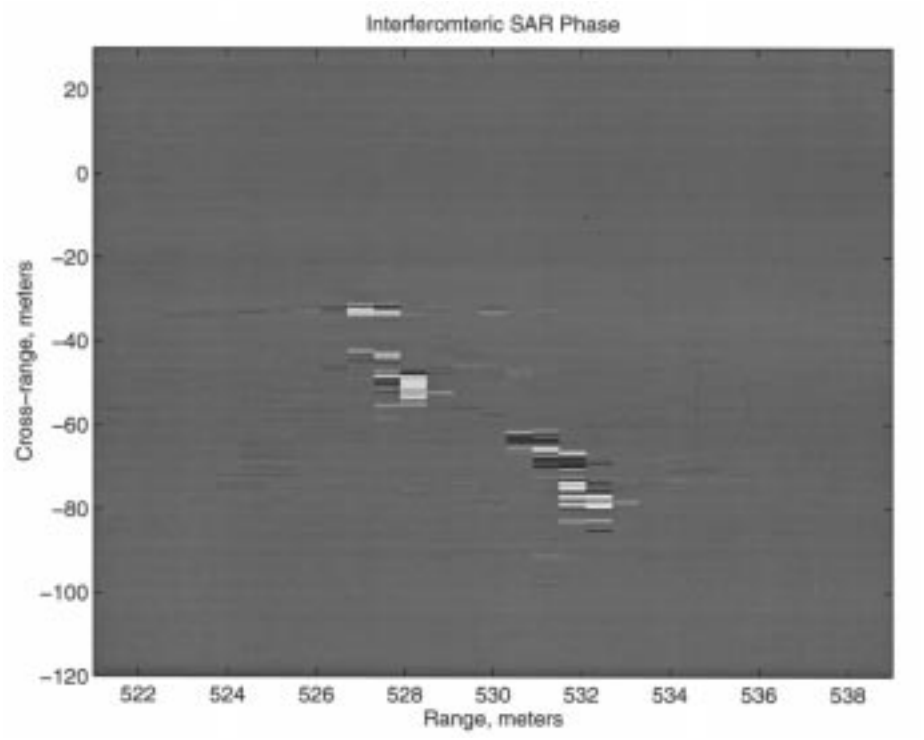

(a)

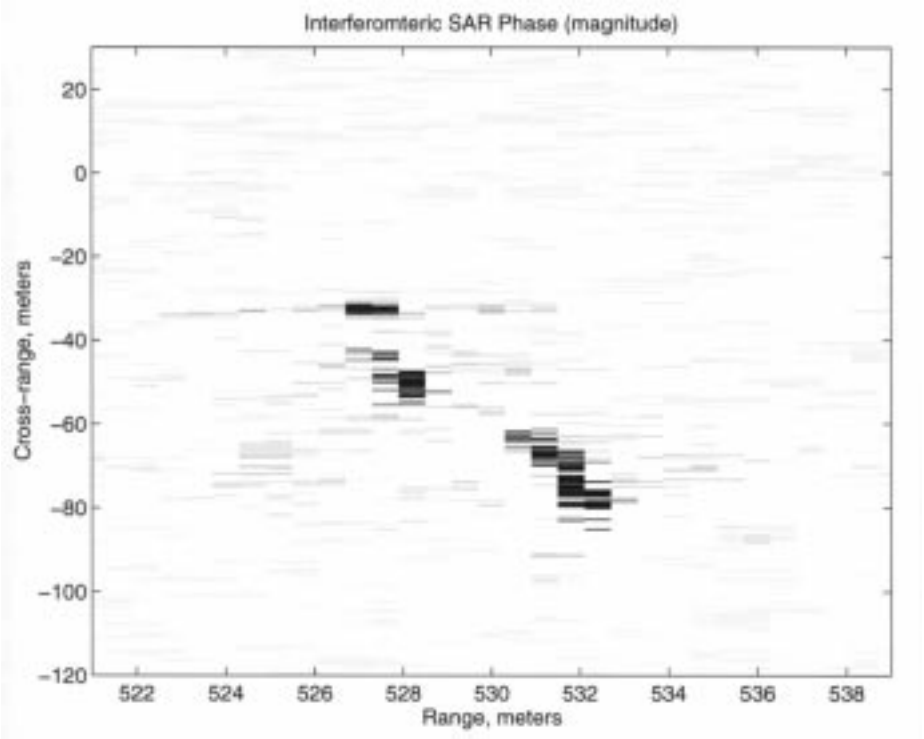

(b)

Fig. 5. Linear motion. (a) Interferometric SAR phase (signed value). (b) Interferometric SAR phase (absolute value).

m. However, its contribution in the difference and interferometric reconstructions of Figs. 4 and 5 is negligible. The dominant phase term for this target is due to by since $a = 0$; the resultant phase term in (15) or (17) is negligible.

Target 3, with $(v_x, v_y) = (4, 0)$ m/s, appears as a solid structure (similar to the surrounding tree trunks) at $(X, Y) \approx (X_m, Y_m/\alpha) = (527.4, -33)$ m. For this target, the dominant phase term in (15) or (17) is due to ax. The target does appear in both the difference reconstruction (see Fig. 4) and the interferometric phase reconstruction (see Fig. 5). Finally, Target 4, with $(v_x, v_y) = (6, 8)$ m/s and $(X_m, Y_m/\alpha) = (532.5, -79.6)$ m, appears at the region $X \in [530, 534]$ m

and $Y \in [-95, -60]$ m. This target is also observable in both Figs. 4 and 5.

IV. Effects of Variations in Altitude and Nonlinear Motion

Next, we consider the 3-D spatial domain, which is encountered in the slant-plane SAR imaging systems. In this model, we also incorporate the effects of maneuvering in a target's motion which is represented as a nonlinear motion model. We use the altitude of the aircraft as the reference $z = 0$ plane; i.e., the coordinates of Radar 1 are $(0, u, 0)$, and the coordinates of Radar 2 are $(0, u - 2\Delta, 0)$ in the 3-D spatial domain.

We identify the 3-D target motion model as a function of the slow-time domain, which includes its nonlinear motion as well as variations in the terrain's altitude, by the following:

$$[x - A(u), y - B(u), z - C(u)]$$

where (x, y, z) are the coordinates of the target at the slow-time $u = 0$ in the 3-D spatial domain; all the parameters and functions in the above model are unknown. For the model in the previous section, we used $A(u) = au$, $B(u) = bu$, and $z = C(u) = 0$.

For this motion model, the monostatic and bistatic round trip distances for a moving target is shown in (20), at the bottom of the page. Since the speed of a ground moving target is much smaller than the speed of the radar-carrying aircraft and the terrain altitude variations on the road that the target moves on are unlikely to be rapid, we can write the following for the derivatives of the motion model:

$$|A'(u)|, |B'(u)|, |C'(u)| \ll 1.$$

Using this fact and $\Delta \ll R$, we can obtain the following approximation:

$$\begin{aligned} &r_m[x + A'(u)\Delta, y + B'(u)\Delta, z + C'(u)\Delta, u) \\ &\quad \approx r_b(x, y, z, u + \Delta) - \frac{\Delta^2}{2R}. \end{aligned} \tag{21}$$

Using (21), one can show that the true monostatic SAR signal $s_m(u, \omega)$ and the synthesized monostatic SAR signal $\hat{s}_m(u, \omega)$ differ by the following phase function:

$$\begin{aligned} &s_m(u, \omega)\hat{s}_m^*(u, \omega) \approx \\ &\quad \exp\left[j2k\Delta\frac{A'(u)x + B'(u)y - B'(u)u + C'(u)z}{R}\right]. \end{aligned} \tag{22}$$

Approximations in (21) and (22) are used to quantify the phase difference between the monostatic and bistatic SAR signatures of the target. However, the fact remains that there is a phase difference between the two measurements which depends on the relative values of the target's parameters and the radar's frequency; this phase function can be significant or negligible. For the latter case, the difference reconstruction or the interferometric phase can be used to detect moving targets.

We associate a zero-mean Gaussian random motion with standard deviation of 0.5 m in the slant-range and cross-range domains to the linear motion of the targets in Table I; the same random motion is used for all four targets. Fig. 6(a) and (b), respectively, show the monostatic and bistatic reconstructions in the close-up target area. Due to the smearing caused by the nonlinear motion, it is difficult to distinguish three of the targets in these images. Fig. 7 shows the difference reconstruction of the images. All targets exhibit some kind of signature in the difference image though Target 2's contribution is marginal. Fig. 8(a) and (b) showS the signed and absolute values of the interferometric SAR phase, respectively. Due to the weak signatures of the targets, which is caused by the nonlinear motion, Targets 2 and 3 are not quite observable (i.e., they do not quite exhibit the visible smearing signatures) in the interferometric images of Fig. 8.

V. Target Motion Parameters Estimation

After a moving target is detected, the next task is to determine its motion parameters. Consider the simpler case of a target moving with a constant velocity on a constant z plane. We mentioned earlier that the bistatic SAR image of a moving target, $f_b(X, Y)$, is a shifted version of its monostatic SAR image, $f_m(X, Y)$ [see (16)]. The shift, i.e., $(a\Delta, b\Delta/\alpha)$, depends on the target's motion parameters. If the user had the tools to measure this shift accurately, the target's motion parameters could be estimated.

Correlating the two images around the smeared monostatic and bistatic images of a detected moving target, and estimating the shift from the peak of the correlated image does not work in practice. This is due to the fact that the amount of shift is smaller than the range and cross-range resolution in most practical reconnaissance SAR problems. A more viable option is to determine the phase of the correlated image in the spatial frequency $k_X, k_Y)$ domain. Unfortunately, this approach also fails since the two smeared images of the moving target are highly contaminated by the focused (strong) images of the surrounding stationary foliage. (2-D spectral estimation methods also fail, since the spectrum of the foliage is unknown and unpredictable.)

There are methods that utilize the phase or instantaneous frequency of a moving target's SAR signature $s(u, \omega)$ in the slow-time domain to estimate its motion parameters, e.g., [4], [17], [18]. These methods can also be used to estimate (a, b) of a moving target with a constant velocity, or $[\sqrt{A'^2(u) + C'^2(u)}, B'(u)]$ for the target model of Section IV. However, these methods are also susceptible to the additive foliage signature.

$$\begin{aligned} r_m(x, y, z, u) \equiv \quad & 2\sqrt{[x - A(u)]^2 + [y - B(u) - u]^2 + [z - C(u)]^2} \\ r_b(x, y, z, u) \equiv \quad & \sqrt{[x - A(u)]^2 + [y - B(u) - u]^2 + [z - C(u)]^2} \\ & + \sqrt{[x - A(u)]^2 + [y - B(u) - u + 2\Delta]^2 + [z - C(u)]^2} \end{aligned} \tag{20}$$

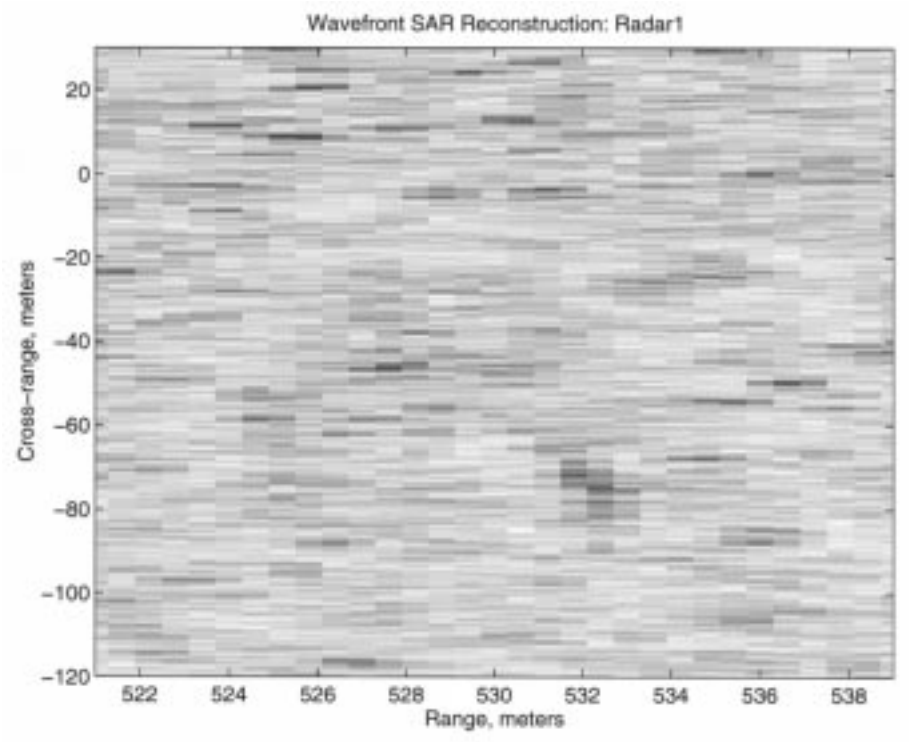

(a)

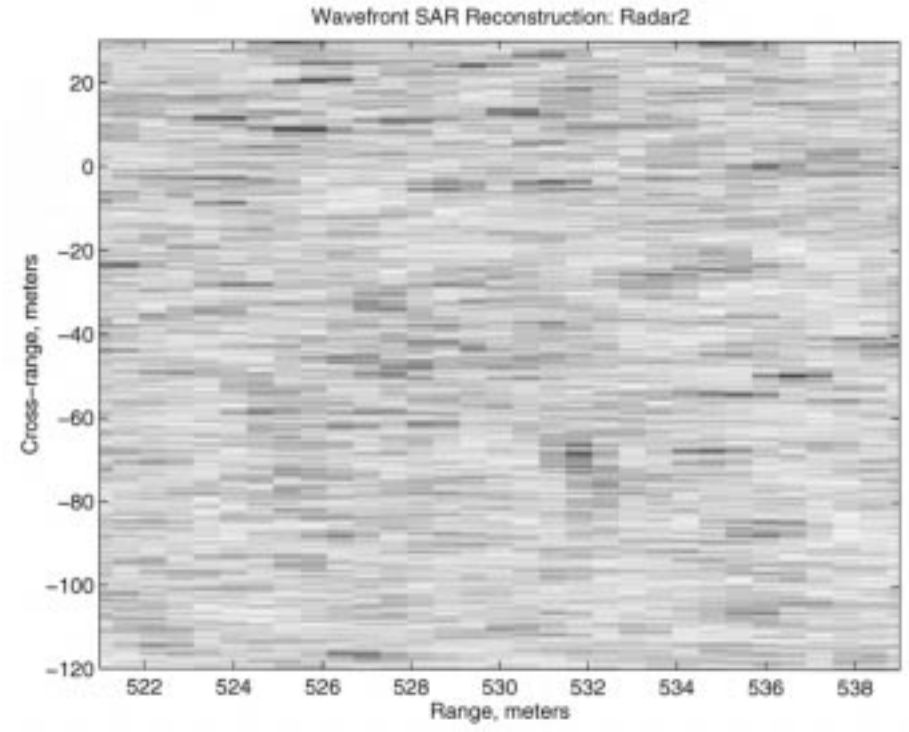

(b)

Fig. 6. Nonlinear motion. (a) Monostatic SAR reconstruction in the close-up target area. (b) Bistatic SAR reconstruction in the close-up target area.

As we mentioned earlier, the contribution of the foliage signature in the difference image, $f_d(X, Y)$, is negligible provided that $\Delta \ll R$. Fig. 9 shows the difference SAR signature, call it $s_d(u, \omega)$, at the fast-time frequency 285 MHz, which is reconstructed from the difference image of Target 4 (with linear motion) via the inverse of the SAR reconstruction algorithm. Fig. 10 is the SAR ambiguity function of this signature [20]. This ambiguity function indicates a peak around $\alpha \approx 1.1$. Thus, the user can obtain an estimate of the target's relative speed (i.e., $\alpha = 1.106$) from the SAR ambiguity function of the foliage-free difference signature.

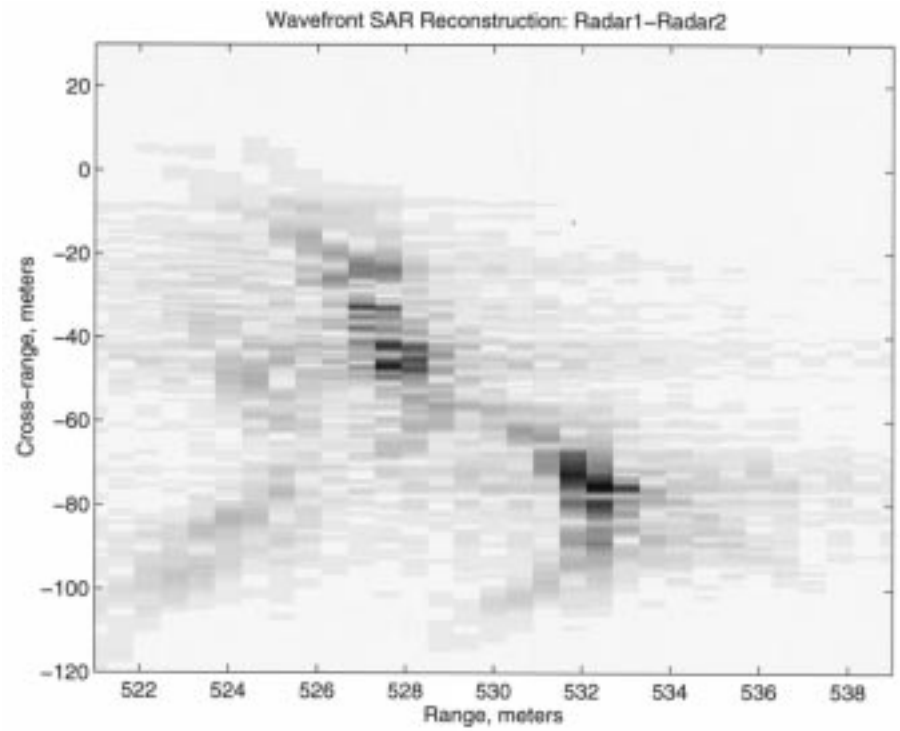

Fig. 7. Nonlinear motion: difference SAR reconstruction in the close-up target area.

Fig. 11(a) is the monostatic SAR image of the target scene, which is obtained by assuming that the aircraft speed is $1.1v_R$ [20]; Fig. 11(b) is the image of the close-up target area. Note that all targets in the scene appear smeared except for Target 4. The bistatic SAR image with $\alpha = 1.1$, which is not shown, exhibits the same phenomenon. The focused image of Target 4 around $(X, Y) = (532.5, -80)$ m does contain some contribution from the smeared foliage signature. However, the power of the target signature to the power of the foliage signature is much higher than the same power ratio for the reconstructed images with $\alpha = 1$.

Fig. 12(a) and (b), respectively, shows the monostatic and bistatic SAR signatures of Target 4, which are obtained from its SAR images with $\alpha = 1.1$, at the fast-time frequency 285 MHz. Using the instantaneous frequency of these two SAR signatures within the fast-time frequency band [250, 350] MHz, the target's velocity is estimated to be $(v_x, v_y) = (5.96, 7.72)$ m/s. A similar estimate is obtained using the spatial frequency phase of the correlated images.

As we mentioned earlier, the instantaneous frequency of a moving target's SAR signature may also be used to estimate its nonlinear motion [18]. However, the limited region of observability of a moving target's SAR signature, which is represented via the Gaussian beam with standard deviation 50 m in our examples, is a major impasse in estimating the target's nonlinear motion parameters. Unfortunately, this is a limiting feature of the UHF stripmap (side-looking) SAR systems, which are used for reconnaissance. The only parameter that one could fairly estimate is the linear component of a moving target's velocity. For the example of Fig. 6, the linear component of Target 4's velocity is estimated to be $(v_x, v_y) = (5.23, 11.87)$ m/s.

VI. Conclusions

This paper analyzed the along track monopulse SAR images of moving targets. Methods for moving target detection in foliage using along track monopulse SAR images were developed. The merits of the methods in detecting moving targets that possessed linear and nonlinear motion were studied. The difference reconstruction exhibited reliable information for moving target detection in both cases. When the moving target signature is severely smeared and is below the foliage signature, the interferometric phase is dictated by the foliage signature. In this case, the interferometric processing and noncoherent methods fail. The same is not true for the coherent difference reconstruction provided that the moving target signature is above the quantization noise of the fast-time analog-to-digital converter; i.e., the moving target signature is in the measured discrete data, though it is dominated by the foliage signature. We close this paper with comments on detection and estimation performance in this system, and future extension of our work.

A. Detection Performance

The main objective of the paper is to present a processing of along track monopulse SAR data that yields removal of stationary targets' signature (i.e., difference and interferometric images). The resultant data base is the input for the manual supervision or the machine-based image processing tool to detect moving targets in the scene. The true performance of this procedure (probabilities of detection, P_D, and false alarm, P_F) can only be established with realistic SAR data. In fact, the theoretical (P_D, P_F) are too good to be true. For the case of coherent clutter (e.g., trees), since the difference image

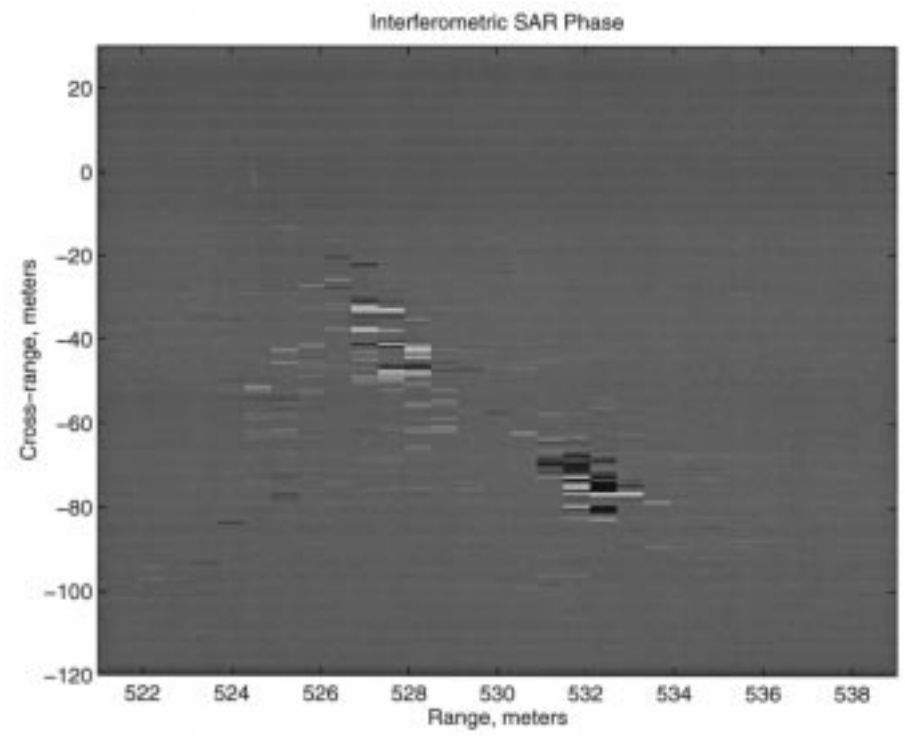

(a)

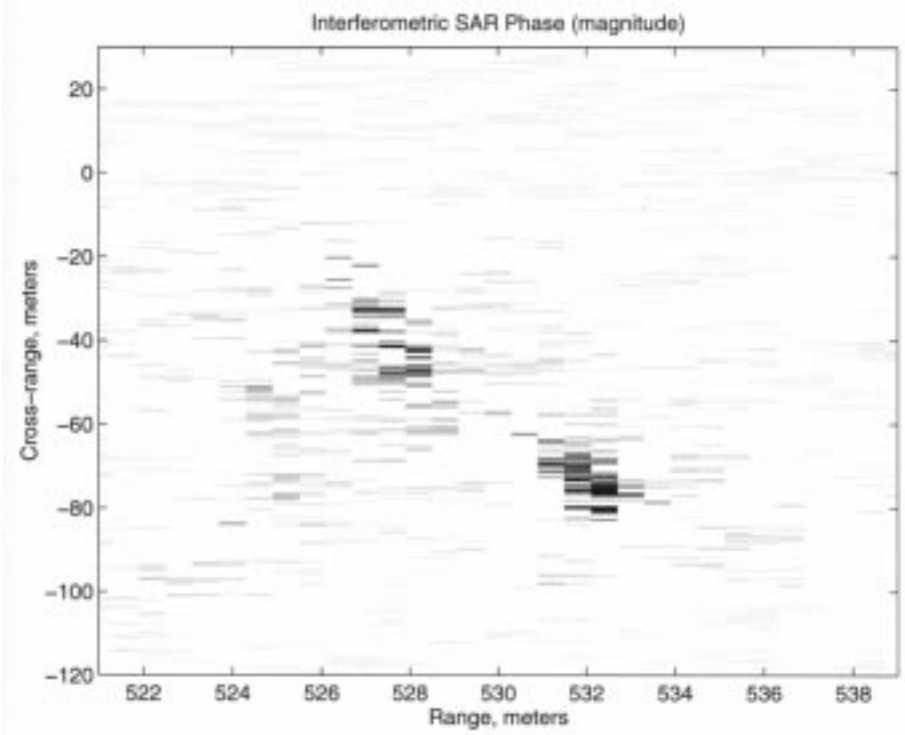

(b)

Fig. 8. Nonlinear motion. (a) Interferometric SAR phase. (b) Interferometric SAR phase (magnitude).

yields a database with no coherent clutter (in theory), thus, $P_D = 1$ and $P_F = 0$. In the case of noncoherent clutter (e.g., additive noise and numerical errors), if the peak value of the target signature in the difference image is above the background noise, then the detection is made. To determine (P_D, P_F) for this case, one has to assume some kind of distribution for the noncoherent clutter (e.g., Gaussian). Using that distribution, one can compute the variance of the output noise in the SAR image. Then, (P_D, P_F) can be computed using the classical detection results (e.g., the tail of the Gaussian distribution, i.e., the error function). A discussion of and a theoretical analysis on input versus output signal-

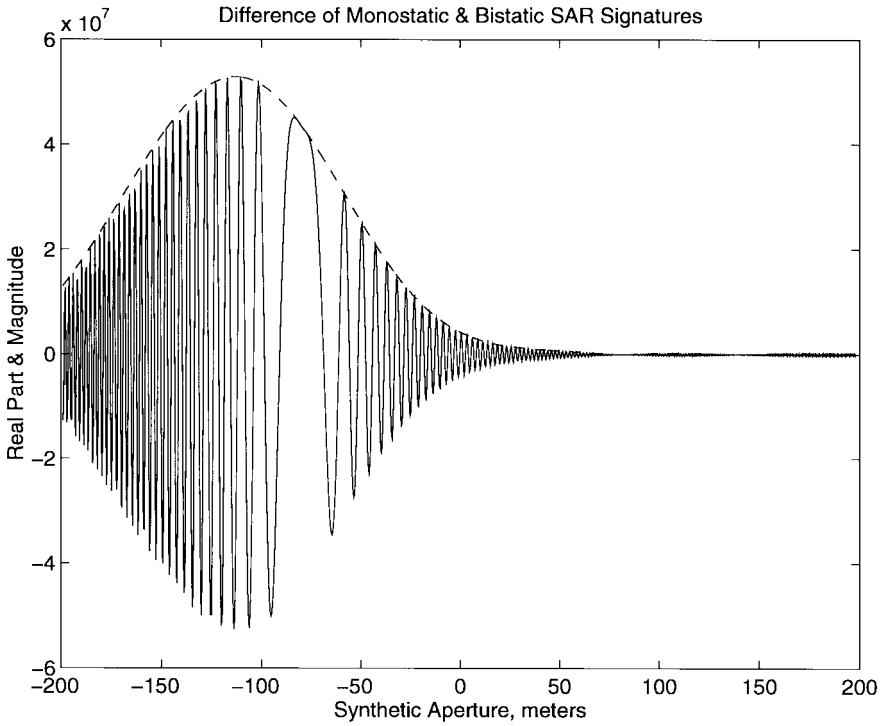

Fig. 9. Difference SAR signature of Target 4 at the fast-time frequency 285 MHz.

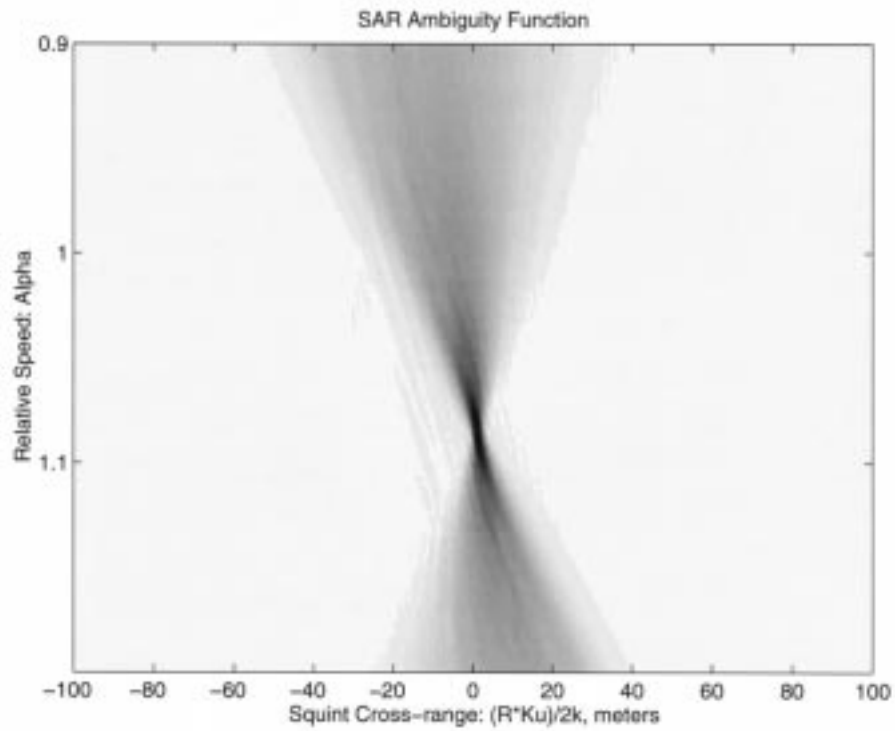

Fig. 10. SAR ambiguity function of SAR signature in Fig. 9.

to-noise (noncoherent/white noise) for SAR/ISAR imaging, in various SAR/ISAR domains and its dependence on the target's parameters (e.g., range and radar cross section) and the noise's variance, are provided in [18, pp. 384–403]. As we pointed out earlier, the true merits of along track monopulse SAR for target detection can only be determined with realistic SAR data.

B. Estimation Performance

Estimating the velocity of a moving target from its SAR or ISAR signature is based on a phase modulation (PM) analysis of its SAR signature (e.g., see [17]). A similar mathematical problem is also encountered in motion compensation in SAR imaging. The general problem is referred to as autofocusing

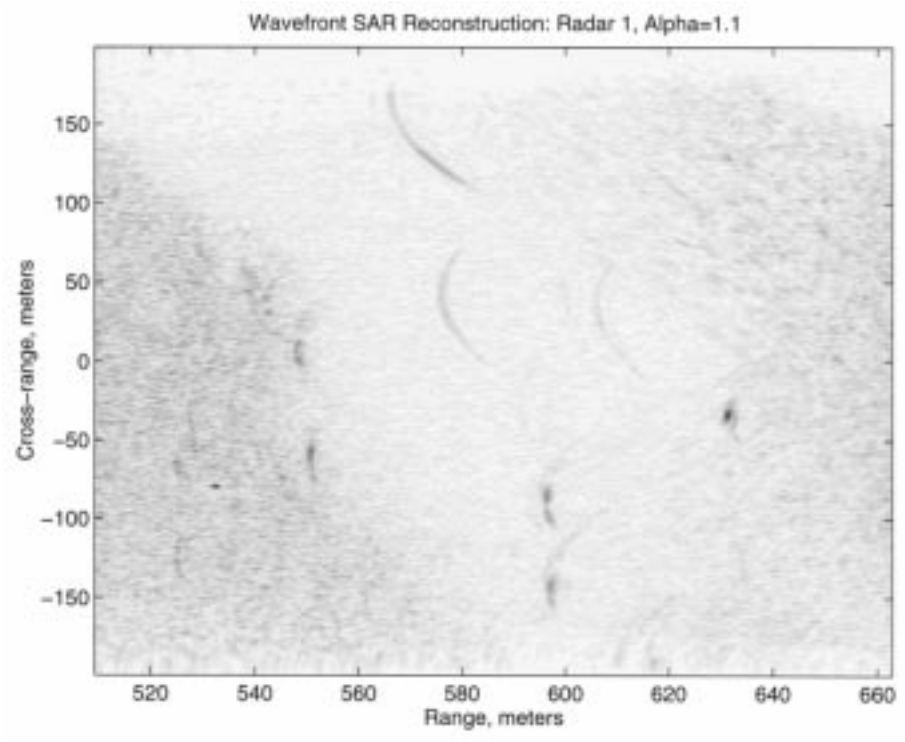

(a)

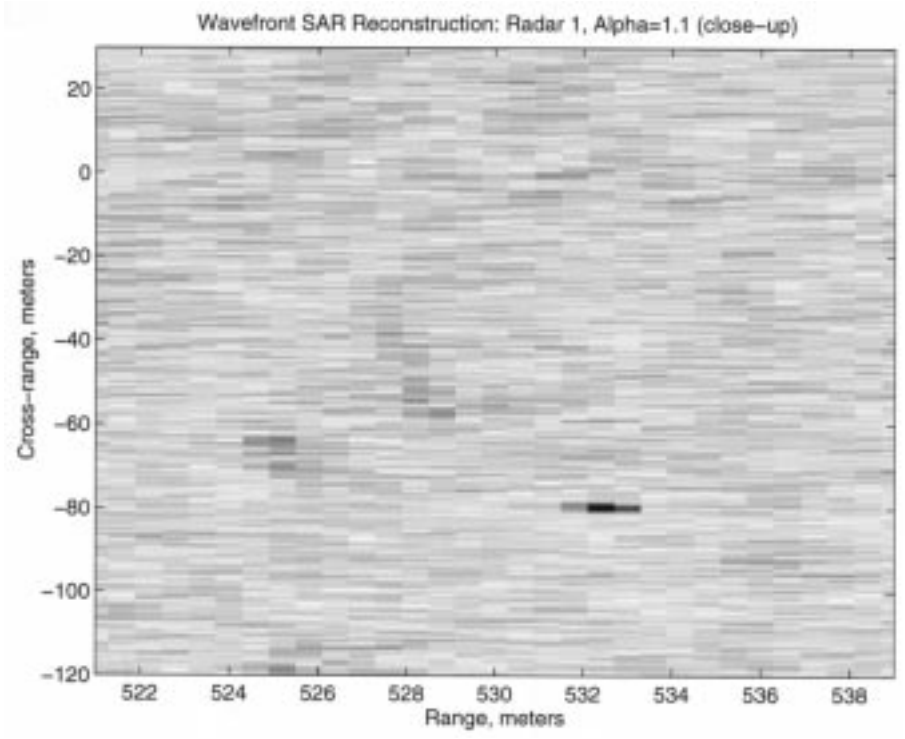

(b)

Fig. 11. (a) Monostatic SAR reconstruction with $\alpha = 1.1$. (b) Close-up of the area where the images of the four moving targets appear.

in the SAR/ISAR community. A recent book [21] provides a complete chapter on various autofocusing techniques, such as, mapdrift and phase gradient autofocus (developed by the Sandia group). All these methods utilize some form of an iterative or noniterative algorithm for recovering a target's slow-time phase history (which contains the target's motion information), however, these methods have not been viewed (or framed) in terms of the well-known maximum likelihood (ML) or *maximum a posteriori* (MAP) multiple parameter estimation methods (e.g., see [22]) where there are well-known constraints and performance equations for the root mean squared (rms) error of an estimator.

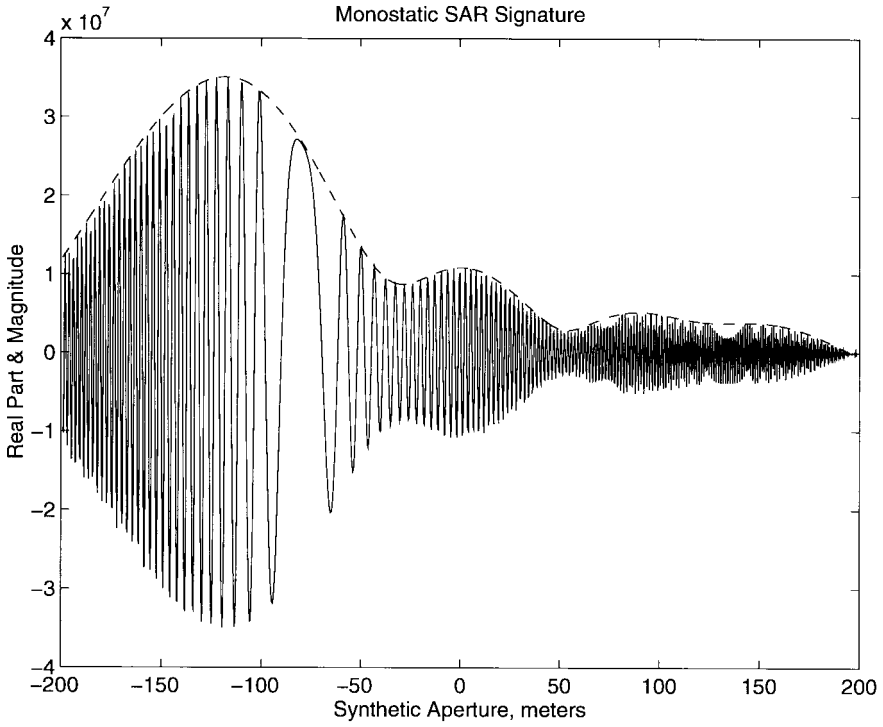

(a)

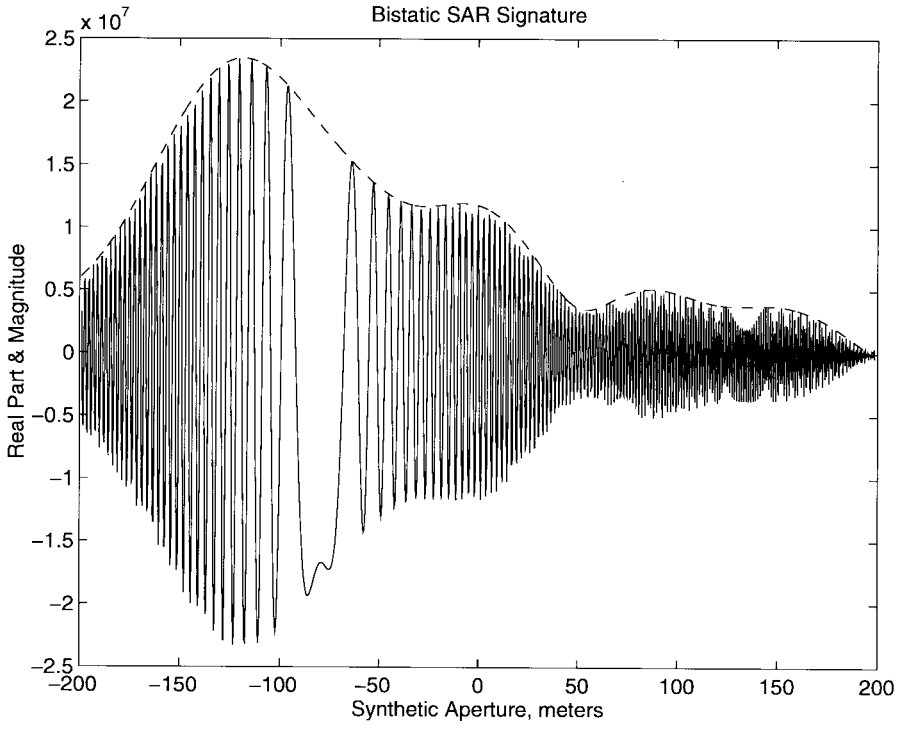

(b)

Fig. 12. (a) Monostatic and (b) bistatic SAR signatures of Target 4.

We brought up the issue of estimating the motion parameters to exhibit the difficult task that the user faces when the target is surrounded by coherent clutter (trees). Once again, one might use classical communication theory principles for estimating the parameters of a phase-modulated signal for a theoretical analysis of the rms error. Clearly, the rms error depends on the noise model (stationary/nonstationary, coherent/noncoherent) and the signal-to-noise ratio. This topic is addressed extensively in classical detection and estimation books [22].

C. Future Work

As we mentioned earlier, difference reconstruction of two or more frames of a scene has been used for noise/clutter

suppression and moving target detection in other coherent and noncoherent imaging modalities, e.g., radar [10]–[12], sonar [13], and IRST [14], [15]. It has been suggested that the performance of the coherent/noncoherent difference reconstruction for clutter filtering can be improved using adaptive least squares differencing, provided that the user has some *a priori* knowledge of the clutter and the additive noise statistics.

ACKNOWLEDGMENT

The author is grateful for the comments and suggestions of the members of Radar Branch and the Technology Research and Development Branch of the Naval Research and Development Laboratory, San Diego, CA.

REFERENCES

[1] M. Pollock, "VHF/UHF ultra-wideband radar for concealed target detection," NCCOSC Tech. Doc., Radar Branch, Nav. Res. and Dev. Lab., 1994.
[2] L. Hoff, "Detection of targets in terrain clutter by using multispectral infrared image processing," in *Proc. SPIE Conf. Signal and Data Processing of Small Targets*, Orlando, FL, Apr. 1991.
[3] R. Raney, "Synthetic aperture imaging radar and moving targets," *IEEE Trans. Aerosp. Electron. Syst.*, vol. AES-7, pp. 499–505, 1971.
[4] S. Barbarossa, "Detection and imaging of moving objects with synthetic aperture radar, Part 1," *Inst. Electr. Eng. Proc.-F*, vol. 139, pp. 79–88, Feb. 1992.
[5] H. A. Zebker and R. M. Goldstein, "Topographic mapping from interferometric synthetic aperture radar observations," *J. Geophys. Res.*, vol. 91, pp. 4993–4999, Apr. 1986.
[6] C. Prati *et al.*, "Seismic migration for SAR focusing: Interferometrical applications," *IEEE Trans. Geosci. Remote Sensing*, vol. 28, pp. 627–640, July 1990.
[7] M. I. Skolnik, *Introduction to Radar Systems.* New York: McGraw Hill, 1980.
[8] B. Edde, *Radar: Principles, Technology, and Applications.* Englewood Cliffs, NJ: Prentice-Hall, 1993.
[9] D. R. Wehner, *High Resolution Radar.* Boston, MA: Artech House, 1987.
[10] B. Cantrell, "A short-pulse area MTI," Rep. 8162, Nav. Res. Lab, Sept. 1977.
[11] A. Leonov and K. Fomichev, *Monopulse Radar,* trans. W. Barton. Boston, MA: Artech House 1986.
[12] S. Sherman, *Monopulse Principles and Techniques.* Boston, MA: Artech House, 1984.
[13] B. Widrow and S. Stearns, *Adaptive Signal Processing.* Englewood Cliffs, NJ: Prentice-Hall, 1985.
[14] R. Fries, "Three dimensional matched filtering," in *Infrared Systems Signal and Components III,* R. Caswell, Ed., vol. 1050. SPIE, Jan. 1989, pp. 19–27.
[15] M. Hartless and J. Barry, "Shipboard infrared search and track," Final Rep. Contract N66001-94-C-6001, NCCOSC, Dec. 1994.
[16] A. Macovski, *Medical Imaging Systems.* Englewood Cliffs, NJ: Prentice-Hall, 1983.
[17] H. Yang and M. Soumekh, "Blind-velocity SAR/ISAR imaging of a moving target in a stationary background," *IEEE Trans. Image Processing,* vol. 2, Jan. 1993.
[18] M. Soumekh, *Fourier Array Imaging.* Englewood Cliffs, NJ: Prentice-Hall, 1994.
[19] ———, "Bistatic synthetic aperture radar inversion with application in dynamic object imaging," *IEEE Trans. Signal Processing,* vol. 39, pp. 2044–2055, Sept. 1991.
[20] ———, "Reconnaissance with ultra wideband UHF synthetic aperture radar," *IEEE Signal Processing Mag.*, July 1995.
[21] W. Carrara, R. Goodman, and R. Majewski, *Spotlight Synthetic Aperture Radar.* Boston, MA: Artech House, 1995, ch. 6.
[22] H. Van Trees, *Detection, Estimation, and Modulation Theory, Parts I–III.* New York: Wiley, 1968.

Mehrdad Soumekh (M'83) received the B.E.E. and Ph.D. degrees from the University of Minnesota, Minneapolis.

He is currently with Lincoln Laboratory, Massachusetts Institute of Technology, Cambridge, on leave from the State University of New York at Amherst, Buffalo, NY. He is a consultant to the government and industry, and served as a faculty fellow at the Naval Command, Control and Ocean Surveillance Center, and the Air Force's Phillips Laboratory. He is the author of *Fourier Array Imaging* (Englewood Cliffs, NJ: Prentice-Hall, 1994).

Dr. Soumekh holds a U.S. patent for his work on Fourier array imaging.